

Article

Design and Analysis of the Two-Impulse Transfer Orbit for a Space-Based Gravitational Wave Observatory

Zhuo Li *, Huixiang Ling and Xiao Zhao

Shanghai Institute of Satellite Engineering, Shanghai 201109, China

* Correspondence: 15046084839@163.com

Abstract: There are plans to set up a space-based gravitational wave observatory that will use an ultra-large-scale laser interferometer in space to detect medium- and low-frequency gravitational waves. Both heliocentric and geocentric formations adopt the method of launching three satellites with one rocket, which has high requirements in terms of the carrying capacity of the rocket. Therefore, a proper transfer design is a prerequisite for achieving space-based gravitational wave detection. In this paper, the transfer orbit for three satellites of the Taiji mission is designed based on the two-impulse transfer model. Moreover, the influence on orbit design of the position of the formation relative to Earth, the initial phase angle of the formation, and the initial time of transfer is analyzed. The Earth-leading and -trailing transfers show opposite patterns in the above three aspects. A smaller velocity increment is required if a proper initial time is selected. After taking into account the stability of the formation, C3, the required velocity increment, transfer time, and the distance to Earth, 20° is determined to be the optimal initial trailing/leading angle.

Keywords: space-based gravitational wave observatory; two-impulse transfer orbit; earth leading/trailing orbit; initial phase angle; transfer time



Citation: Li, Z.; Ling, H.; Zhao, X. Design and Analysis of the Two-Impulse Transfer Orbit for a Space-Based Gravitational Wave Observatory. *Aerospace* **2024**, *11*, 234. <https://doi.org/10.3390/aerospace11030234>

Academic Editor: Hyun-Ung Oh

Received: 31 December 2023

Revised: 10 March 2024

Accepted: 13 March 2024

Published: 16 March 2024



Copyright: © 2024 by the authors. Licensee MDPI, Basel, Switzerland. This article is an open access article distributed under the terms and conditions of the Creative Commons Attribution (CC BY) license (<https://creativecommons.org/licenses/by/4.0/>).

1. Introduction

In 2016, the Laser Interferometer Gravitational Wave Observatory (LIGO) detected gravitational wave signals using a ground gravitational wave observatory for the first time, proving Einstein's prediction of general relativity. Since then, the detection of gravitational waves has become a research hotspot in the fields of physics, astronomy, and aerospace [1,2]. Compared with ground gravitational wave observatories, space-based gravitational wave observatories could utilize ultra-large-scale laser interferometers in space free from the interference of ground noise and the influence of the Earth's curvature to detect medium- and low-frequency gravitational waves. Space-based gravitational wave detection will greatly enrich the wave sources.

The current main domestic and foreign space-based gravitational wave observatories include the Laser Interferometer Space Antenna (LISA) launched jointly by NASA and the ESA, the Taiji program proposed by the Chinese Academy of Sciences, and the TianQin project initiated by Sun Yat-Sen University. Each of the three missions consists of three satellites, which constitute an ultra-large-scale formation. Each satellite carries two test masses, between which laser beams transfer information. When gravitational waves pass through the laser beams, the laser interferometer records the changes in the optical path. In the LISA [3–6] and Taiji [7–10] missions, the three satellites sit in a heliocentric orbit, leading or trailing the Earth by around 20° , forming an equilateral triangle with side lengths of $2.5\text{--}3.0 \times 10^6$ km. In the TianQin mission, the three satellites are located in a geocentric orbit 10^5 km away from Earth, forming an equilateral triangle with side lengths of 1.7×10^5 km [11–15]. Each satellite is approximately 1.5 tons in weight. Both heliocentric and geocentric formations adopt the method of launching three satellites with one rocket, which has high requirements in terms of the carrying capacity of the rocket.

Therefore, a proper transfer design is a prerequisite for achieving space-based gravitational wave detection.

There is research on the design of a transfer orbit for space-based gravitational wave observatories. Xia [16] discussed the problems of transfer orbit design for the LISA mission and finally provided a plan. That is, the three satellites were first sent to the virtual center for formation configuration in space. Then, they separated from each other, changed their orbits, and transferred to their respective target positions, forming the original formation. Sweetser [17] also designed a transfer orbit for the LISA mission and suggested that the three satellites should be launched by one rocket at a time to the target orbit, leading the Earth by 20° (this process would last a year and a few weeks). Different from Xia's plan, in Sweetser's design, the three satellites separated from each other shortly after the launch and transferred to their respective target orbits. Meanwhile, Joffre [18] explored the launch problem in the LISA mission and investigated different types of stable formations, such as clockwise, counterclockwise, leading, and trailing orbits. He advised that the selection of the original formation should take scientific requirements, the impact of the Earth, and feasibility into account. Wang et al. [19] studied the orbit design of B-DECIGO and DECIGO and compared the amount of fuel consumed to form the original formation among B-DECIGO, DECIGO, LISA, and Taiji. Wu et al. [20] designed a transfer orbit for rocket-satellite separation in the formation generation of the ASTROD-GW mission. They proposed using a two-impulse strategy to control the Hohmann transfer of the three satellites to libration points L3 to L5. Hellings et al. [21] investigated the initialization of the formation of the OMEGA task. They suggested that the three satellites should be transferred to the target orbit through a low-energy transfer method like that used in the GRAIL mission. Then, upper-stage deceleration should be performed to lower the perigee of the orbit and promote the generation of a stable formation. Giulicchi et al. [22] introduced the control system of LISA Pathfinder. A comprehensive attitude and orbit control system first lifted the low Earth orbit 10 consecutive times so that the satellites could enter the target orbit. After the propulsion module was discarded, a micro-propulsion system took over, and scientific exploration was finally fulfilled via a drag-free control system. In addition, Zhang et al. [23] discussed the initialization problem of near-Earth and small space-based gravitational wave observatories, explored the globally optimal differential correction strategy, and constructed a high-precision formation.

In this paper, the transfer orbits of three satellites of the Taiji mission are designed based on the two-impulse transfer model. Moreover, the influence of the position of the formation relative to the Earth, the initial phase angle of the formation, and the initial time of transfer in relation to orbit design are analyzed. This is the first study on the transfer orbit design of China's heliocentric orbit space gravitational wave observatory, and scientists of the Taiji team may use the results of this paper to optimize the orbit design.

2. Dynamic Model

2.1. Two-Impulse Transfer Orbit Model for Space-Based Gravitational Wave Observatory

The transfer process of satellites from launch to arrival at the target orbit is shown in Figure 1. The three satellites are launched simultaneously. Shortly after they leave the rocket, they are separated from each other and then move to their target orbit. We suppose that at the initial time, the satellites are located in a 200 km high parking orbit. The segment of orbit located within the sphere of influence of the Earth is a coasting section. The residual velocity of the hyperbola is V_∞ when it reaches the edge of the sphere of influence of Earth. All three satellites enter their target orbits in the manner of Lambert transfer. The processes are transformed into optimization problems of six variables, which are escape velocity increment V_∞ , escape azimuth angle A_z , escape pitch angle A_E , coasting time $\Delta T1$, Lambert transfer time $\Delta T2$, and phase angle of the formation α . In the coasting section, the satellites are located in the sphere of influence of Earth and thus are affected by the gravity of the Sun and Earth. The recursive model for the transfer orbit in the geocentric coordinate system is shown in (1). After leaving the coasting section in the

sphere of influence of Earth, the satellites enter the Lambert transfer section. The problem is solved in the heliocentric coordinate system. In addition, the target formation status needs to be solved as the destination of the Lambert transfer. The whole optimization process is illustrated in Figure 2. $\Delta V1$ is the velocity increment of the satellite from the coasting section to the Lambert transfer section. $\Delta V2$ denotes the velocity increment of the satellite from the end of the Lambert transfer section and the target orbit.

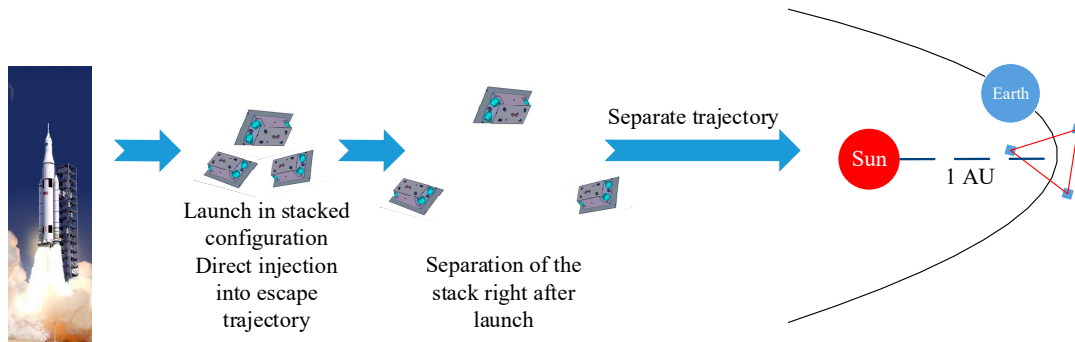


Figure 1. The launch and transfer process.

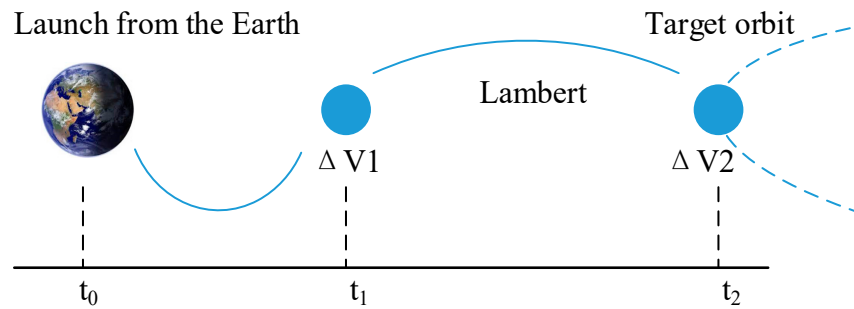


Figure 2. The two-impulse transfer process.

In the geocentric J2000 coordinate system, the satellite is subjected to the central gravity of the Earth and the perturbation forces of the Sun and Moon, $\mathbf{a}_{Satellite} = \mathbf{a}_{Earth} + \mathbf{a}_{Sun} + \mathbf{a}_{Moon}$, the dynamic model of the coasting section is expressed in detail as:

$$\ddot{\mathbf{r}}_k = -\mu_E \frac{\mathbf{r}_k}{r_k^3} - \mu_S \left(\frac{\mathbf{R}_S}{R_S^3} + \frac{\mathbf{r}_k - \mathbf{R}_S}{|r_k - R_S|^3} \right) - \mu_M \left(\frac{\mathbf{R}_M}{R_M^3} + \frac{\mathbf{r}_k - \mathbf{R}_M}{|r_k - R_M|^3} \right) \quad (1)$$

where \mathbf{r}_k is the position vector of the three satellites, $k = 1, 2, 3$; \mathbf{R}_S and \mathbf{R}_M are the position vectors of the center of the Sun and the center of the Moon, respectively; μ_E , μ_S and μ_M are the gravitational constants of Earth, Sun, and Moon, respectively.

\mathbf{V}_∞ is the velocity of the satellite relative to the Earth when it leaves the Earth. δ and α are the right ascension and declination of \mathbf{V}_∞ . T and R are the B-plane parameters of the satellite's transfer to the target orbit, which describe the two fundamental axes. θ_∞ represents the angle between vector B and axis T . μ is the coefficient of gravity, \hat{h} is the momentum moment of the hyperbolic orbit, and \mathbf{V}_{Vp} is the perigee velocity of the hyperbola.

The perigee velocity of the hyperbolic transfer orbit during the optimization process is calculated by:

$$\mathbf{S} = \frac{\mathbf{V}_\infty}{V_\infty} = [\cos \delta \cos \alpha \quad \cos \delta \sin \alpha \quad \sin \delta]^T \quad (2)$$

$$\mathbf{T} = \mathbf{S} \times [0 \ 0 \ 1]^T, \mathbf{R} = \mathbf{S} \times \mathbf{T} \quad (3)$$

$$\cos \theta = \frac{\cos i}{\cos \delta}, \sin \theta = -\sqrt{1 - \cos^2 \theta} \tag{4}$$

$$\mathbf{h} = T \sin \theta - R \cos \theta, \hat{h} = \frac{\mathbf{h}}{h} \tag{5}$$

$$\cos \theta_\infty = -\frac{\mu}{r_p V_\infty^2 + \mu}, \sin \theta_\infty = \sqrt{1 - \cos^2 \theta_\infty} \tag{6}$$

$$\mathbf{V}_{rp} = S \cos \theta_\infty - (\hat{h} \times S) \sin \theta_\infty, \hat{\mathbf{V}}_{rp} = \frac{\mathbf{V}_{rp}}{V_{rp}}, \mathbf{R}_p = \hat{\mathbf{V}}_{rp} r_p \tag{7}$$

$$\mathbf{V}_p = \sqrt{\frac{2\mu}{r_p} + V_\infty^2}, \mathbf{V}_{Vp} = \hat{h} \times \mathbf{V}_{rp}, \hat{\mathbf{V}}_{vp} = \frac{\mathbf{V}_{Vp}}{V_{Vp}}, \mathbf{V}_p = \hat{\mathbf{V}}_{vp} V_p \tag{8}$$

where α and δ are the right ascension and declination of \mathbf{V}_∞ .

2.2. Formation Flying Model of the Space-Based Gravitational Wave Observatory

In the LVLH coordinate system, the relative position and velocity are expressed as:

$$\ddot{x} - 2\dot{\theta}y - \dot{\theta}^2 x - \ddot{y} = -\frac{\mu(r+x)}{[(r+x)^2 + y^2 + z^2]^{\frac{3}{2}}} + \frac{\mu}{r^2} \tag{9}$$

$$\ddot{y} + 2\dot{\theta}x - \dot{\theta}^2 y + \ddot{x} = -\frac{\mu y}{[(r+x)^2 + y^2 + z^2]^{\frac{3}{2}}} \tag{10}$$

$$\ddot{z} = -\frac{\mu z}{[(r+x)^2 + y^2 + z^2]^{\frac{3}{2}}} \tag{11}$$

where μ is the gravitational constant; r is the radial distance from the satellites to the virtual center (in the LVLH coordinate system, three satellites make up a circle, the center of the circle is defined as the virtual center); and the argument of latitude is $\theta = \omega + f$.

The above formula is transformed into magnitude and phase representations as follows:

$$\begin{cases} x(t) = -\frac{1}{2}r_{xy} \cos(nt + \theta_{xy}) \\ y(t) = r_{xy} \sin(nt + \theta_{xy}) + y_{off} \\ z(t) = -r_z \cos(nt + \theta_z) \end{cases} \tag{12}$$

$[r_{xy}, r_z, \theta_{xy}, \theta_z, y_{off}]$ are the design parameters of the formation, from which we derive the stable heliocentric formation with the side length of 3×10^6 km leading or trailing the Earth by 20° .

2.3. Constraints on Formation Design for Space-Based Gravitational Wave Observatory

In order to ensure the stability of the constellation, the constellation must be away from the gravitational disturbance of the Earth–Moon system. However, as the distance from the Earth increases, the difficulties of deep space measurement and control, data transmission, and automatic laser acquisition between satellites increase, so the distance from the constellation to the Earth is generally limited to 6.5×10^7 km.

The choice of the arm length of laser interferometry directly affects the sensitive frequency band and determines the main wave source type. In Taiji, the key research object is the intermediate mass binary black hole merging system, weighing several hundred to one hundred thousand solar masses, and the key detection frequency band is 0.01 to 1 Hz, so the arm length is selected to be 3×10^6 km.

The change rate of the arm length affects the Doppler shift between the laser receiving and transmitting beams, and 1 m/s corresponds to 1 MHz Doppler shift for the wavelength chosen by Taiji. The Doppler shift is limited to ± 10 MHz, so the arm length change rate is

within 10 m/s. The size of the breathing angle affects the pointing accuracy of the telescope, as well as small angular changes between the incoming and outgoing beams. The range of the breathing angle does not exceed 1° .

During the task, the arm length indicators should change by no more than 35,000 km, the breathing angle by no more than 1° , the rate of change in the arm length by no more than 10 m/s, and the distance between the satellite and the Earth should generally be no more than 6.5×10^7 km.

3. Principle of NSGA-II Algorithm

For the space-based gravitational wave observatory, in addition to the fuel consumption constraint during the transfer process, there are also requirements relating to the transfer time. It is hoped that the fuel consumption in the transfer process will be as small as possible, and that the transfer time will not exceed 1.5 years. Therefore, this paper adopts a multi-objective optimization method, in which one optimization objective is fuel consumption and the other objective is transfer time. After the optimization, multiple sets of feasible solutions are given, and the Taiji team scientists can choose the appropriate solution according to these solutions.

The conventional method for solving multi-objective optimization problems is to combine multiple objective functions into one. This method relies on the selection of weights, which affects the decision outcome. By contrast, multi-objective optimization algorithms provide a set of feasible solutions for the decision maker, who is able to select the solution according to the needs.

Deb proposed the non-dominated sorting genetic algorithm (NSGA), which sorts individuals based on the dominant relationship and then selects individuals. The excellent genes of an individual at a higher level are more likely transferred into the next generation. In addition, a virtual fitness value is assigned to each level of NSGA so that individuals at higher levels are selected for the creation of the next generation. In this way, the algorithm can converge quickly.

Later, Deb improved the NSGA algorithm and proposed the NSGA-II algorithm with an elite strategy, which made up for the defects of NSGA. The NSGA-II algorithm is simpler than the NSGA algorithm, and preserves the diversity of the population by uniformly distributing the Pareto front. Moreover, the NSGA-II algorithm expands the sampling space, and combines the parent and offspring populations for tournament selection to produce the next population, and to find the optimal solution that may be missed in the parent population.

The basic procedure of NSGA-II to solve a problem is as follows, and is shown in Figure 3:

Step 1: Parameters are initialized, and a random initial population P_t of size N is generated within the specified search range. t represents the t^{th} population and P_t ($t = 0$) is the parent population.

Step 2: Non-dominated sorting and basic genetic operations of the parent population P_t are carried out to produce the offspring population Q_t .

Step 3: The parent and offspring populations are combined to create a new population of size $2N$. Non-dominated sorting is conducted, the crowding distance is calculated, and elitism is performed to select a new parent population of size N for the generation of the next population. We make $t = t + 1$.

Step 4: Selection, crossover, and mutation of the new parent population are performed. Once this is done, we check if the maximum number of evolutions has been reached. If it is, we end the process and take the last population as the optimal solution. Otherwise, we repeat the process from Step 3.

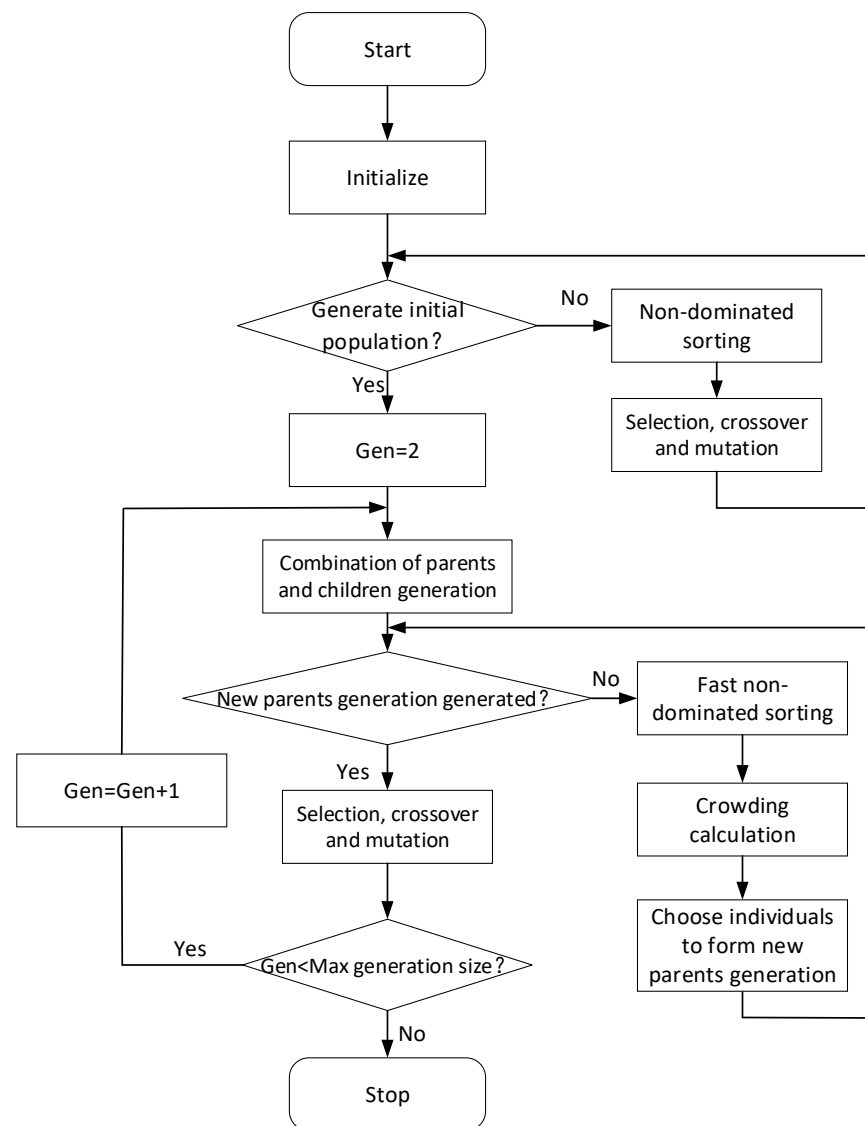


Figure 3. Procedure of NSGA-II.

4. Simulation and Analysis

4.1. Selection of Optimization Objectives

The time spent in the transfer section is required to be less than 1.5 years in space-based gravitational wave detection missions. At the same time, minimal fuel consumption should be taken into account in transfer orbit design in order to extend the lifespan of satellites in orbit. This paper compares the effects of three optimization objectives through simulations. The three objectives are (a) to minimize the total fuel consumption of the formation of satellites, (b) to equalize the fuel consumption of each satellite as much as possible, and (c) to minimize the fuel consumption of each satellite. The two-impulse transfer model is used for simulations and the satellites are set to leave the Earth's parking orbit on 1 April 2027. The optimization results are shown in Table 1. J_1 , J_2 , and J_3 represent different optimization objectives, namely, the minimal total fuel consumption, the most uniform fuel consumption, and the minimal fuel consumption of each satellite. J_1 , J_2 , and J_3 can be expressed as:

$$J1 = \sum_{i=1}^3 J_i \quad (13)$$

$$J2 = \sqrt{\frac{1}{3} \sum_{i=1}^3 (J_i - \bar{J})^2} \quad (14)$$

$$J3 = \max([\Delta V1 \Delta V2 \Delta V3]) \quad (15)$$

Table 1. Results of different optimization objectives.

	$\Delta V1$ (km/s)	$\Delta V2$ (km/s)	$\Delta V3$ (km/s)	Total Velocity Increments (km/s)	Transfer Time (Days)
J1	0.6971	0.8388	0.4800	2.0160	384.7769
J2	1.1260	1.1260	1.1260	3.3780	356.7949
J3	0.7994	0.7994	0.5871	2.1861	390.6246

According to the formula $m_0 = m_t \exp(\Delta V / I_{sp})$, because the three satellites are the same, the initial mass m_0 and the specific impulse I_{sp} of each satellite are the same, and the fuel consumption m_t in the transfer process is positively correlated with ΔV , so the fuel consumption of the three satellites can be compared by ΔV .

$\Delta V1$, $\Delta V2$, and $\Delta V3$ are the required velocity increments of the three satellites during the transfer process. The velocity increments and transfer time of the satellites under the three optimization objectives are summarized in Table 1.

According to Table 1, the total velocity increment of the three satellites is the smallest under the optimization objective of J1. The difference between the maximal and minimal velocity increments of the three satellites is 0.3588 km/s. Under the optimization objective of J2, the velocity increments of the three satellites are almost equal, but significantly larger than those under J1 and J2. Under the optimization objective of J3, the velocity increments of the three satellites are close and the sum is slightly greater than that under J1. Moreover, the transfer time under J3 is the longest, but fuel consumption takes priority over transfer time in the transfer process design. Therefore, J3 is selected as the optimization objective in the following simulation.

4.2. Two-Impulse Transfer Orbit Simulation

The satellites move from the Earth's parking orbit to positions leading and trailing the Earth by 20° . The optimization variables x are escape velocity increment, escape azimuth angle, escape pitch angle, coasting time, Lambert transfer time, and initial phase angle of the formation. Their respective symbols are shown in (16):

$$x = [V_\infty, A_z, A_E, \Delta T_1, \Delta T_2, \alpha] \quad (16)$$

The objective functions are the required maximum velocity increment and transfer time during the transfer process of the three satellites.

$$J1 = \max([\Delta V1 \Delta V2 \Delta V3]) \quad (17)$$

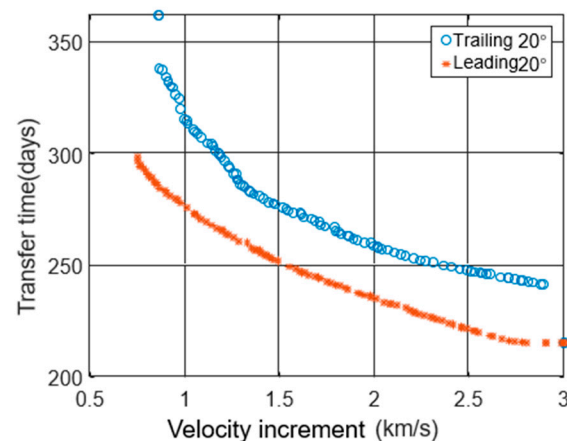
$$J2 = \Delta T_1 + \Delta T_2 \quad (18)$$

The two-pulse transfer model of the space gravitational wave observatory has been established as described above. According to China's launch conditions, the escape velocity increment is not more than 0.6 km/s, the escape azimuth is between 0 and 360° , and the escape pitch angle is not more than 19.5° . The Taiji mission requires the transfer time to be no more than 550 days, so it is hoped that the glide time is no more than 150 days, and the Lambert transfer period is no more than 400 days. The initial phase angle constraint of the constellation is $0 \sim 180^\circ$. The constraints for Taiji two-impulse transfer orbit design are shown in Table 2.

Table 2. Constraints for Taiji two-impulse transfer orbit design.

Constraints	Value
Escape velocity increment	0.1~0.6 km/s
Escape azimuth angle	0~360°
Escape pitch angle	−19.5~19.5°
Coasting time	15~150 days
Lambert transfer time	200~400 days
Initial phase angle of the formation	0~180°

The satellites leave the Earth's parking orbit on 1 April 2026. The Pareto curve of the optimal solutions is shown in Figure 4. In practice, due to the limited capacity of the satellites to carry fuel, the velocity increment should not be too large, so we only consider the situation of a velocity increment less than 1 km/s. When the formation trails the Earth by 20°, the required velocity increment of a single satellite ranges between 0.8582 and 1 km/s, and the transfer time is 315 to 362 days. When the formation leads the Earth by 20°, the required velocity increment of a single satellite is 0.7487 to 1 km/s and the transfer process lasts 276 to 298 days. The initial phase angles of the formation corresponding to the minimal velocity increment of Earth-trailing and -leading transfers are 111° and 83°, respectively.

**Figure 4.** Multi-objective optimization results of two-impulse transfer.

In Figure 4, the launch energy C3 of the minimal velocity increment is taken. The required velocity increments $\Delta V1$, $\Delta V2$, and $\Delta V3$, and the transfer time of the three satellites, are shown in Table 3. In the simulation case of this section, the transfer orbit leading the Earth by 20° can reduce the velocity increment and transfer time, and the transfer orbit trailing the Earth by 20° can save launch energy C3.

Table 3. Results of two-impulse transfer.

	C3	$\Delta V1$ (km/s)	$\Delta V2$ (km/s)	$\Delta V3$ (km/s)	Transfer Time (Days)
Trailing 20°	0.1044	0.8582	0.8581	0.8527	362.0399
Leading 20°	0.3084	0.7482	0.7250	0.7487	298.4096

4.3. Analysis of Factors Affecting Transfer Orbit Design

There are many factors affecting the transfer orbit design. For the problem of space gravitational wave detection, the authors select three of them in this paper: the initial trailing angle, the initial phase angle, the initial time of transfer, and analyze their effects

on the transfer orbit design. Taiji scientists can optimize the transfer orbit design based on the results of this paper.

(1) The effect of the initial trailing angle on the transfer orbit

The trailing/leading angle refers to the angle between the line joining the centers of the Earth and Sun and the line connecting the virtual center of the formation and the center of the Sun (Figure 5). With the increase in the trailing/leading angle from 14° to 22° , the variations in the breathing angle of the formation, the velocity increment required for transfer, the launch energy C3, and the transfer time are shown in Figure 6 (the initial time of transfer is 1 January 2026) and Figure 7 (the initial time of transfer is 1 April 2027).

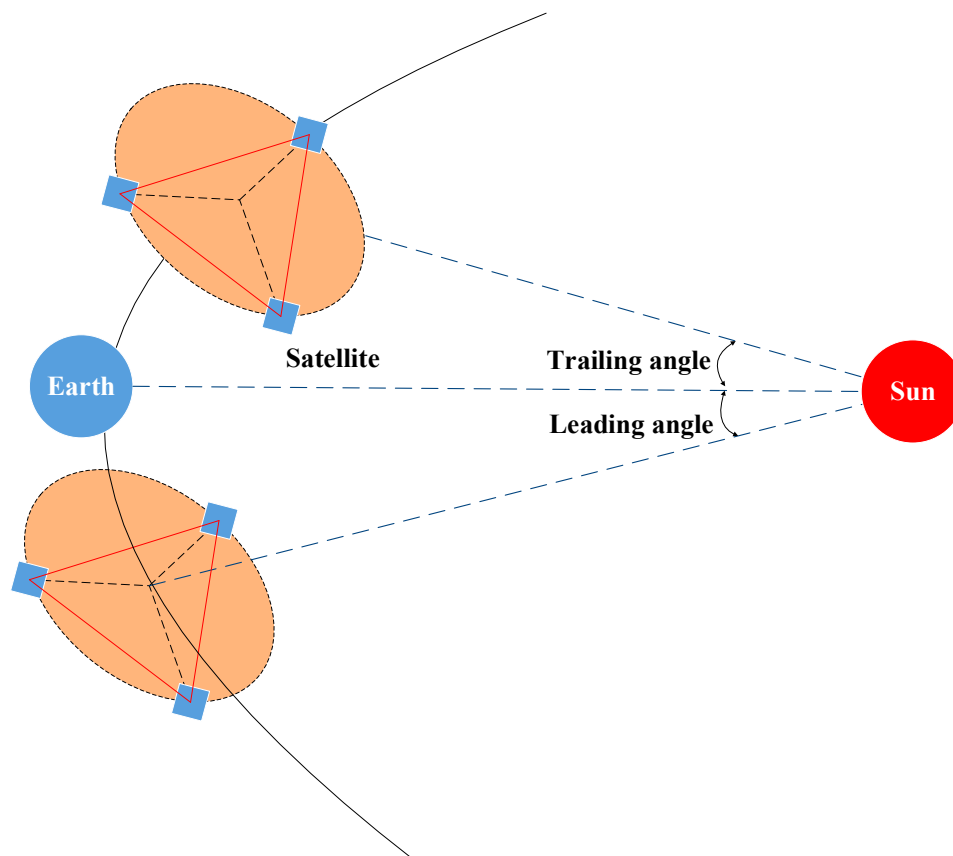


Figure 5. Trailing and leading angle.

It can be seen from Figures 6 and 7 that the breathing angle is significantly affected by the initial trailing/leading angle if it is smaller than 18° . However, an initial trailing/leading angle greater than 18° has a slight influence on the breathing angle. Since it is required that the change in the breathing angle should be within the range of $\pm 1^\circ$, the formation proposed satisfies the requirement if the trailing/leading angle is smaller than 20° . According to Figures 6 and 7b–d, the velocity increment required for transfer, C3, and transfer time increase with the increase in the initial trailing/leading angle, and the increase is significant when the initial trailing/leading angle exceeds 20° . Therefore, a smaller initial trailing/leading angle that satisfies the requirements of formation design is conducive to the launch. However, affected by the attraction between the Moon and Earth, the formation drifts away from the Earth more quickly during the process of completing the mission if the initial trailing/leading angle is too small.

Therefore, the formation with the initial trailing/leading angle of 20° is selected as the goal of the transfer orbit design. It can meet the requirements of both transfer section design and formation design.

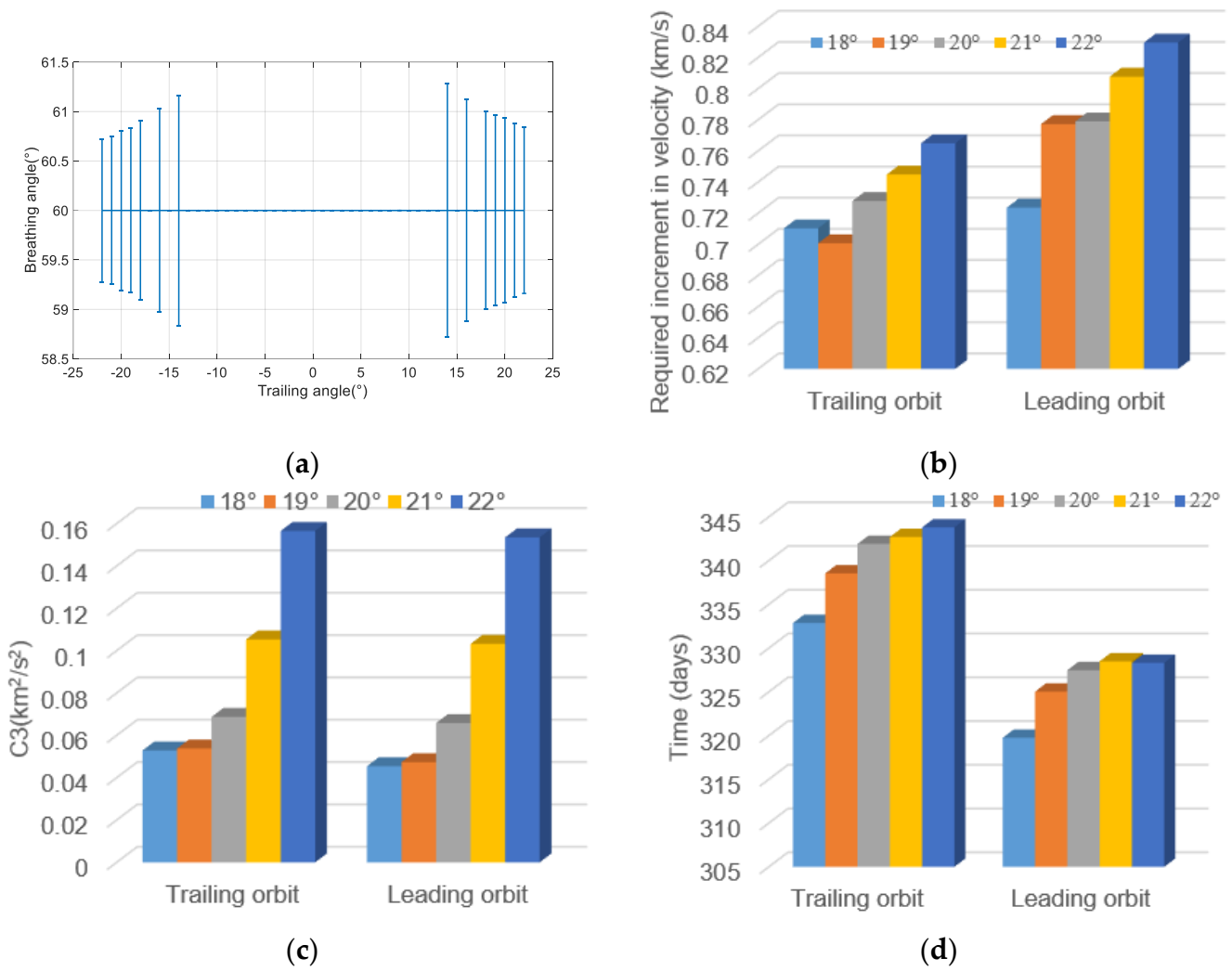


Figure 6. The effect of the initial trailing angle on the transfer orbit (the initial time of transfer is 1 January 2026). (a) The effect of the initial trailing angle on breathing angle; (b) the effect of the initial trailing angle on velocity increment; (c) the effect of the initial trailing angle on C3; (d) the effect of the initial trailing angle on transfer time.

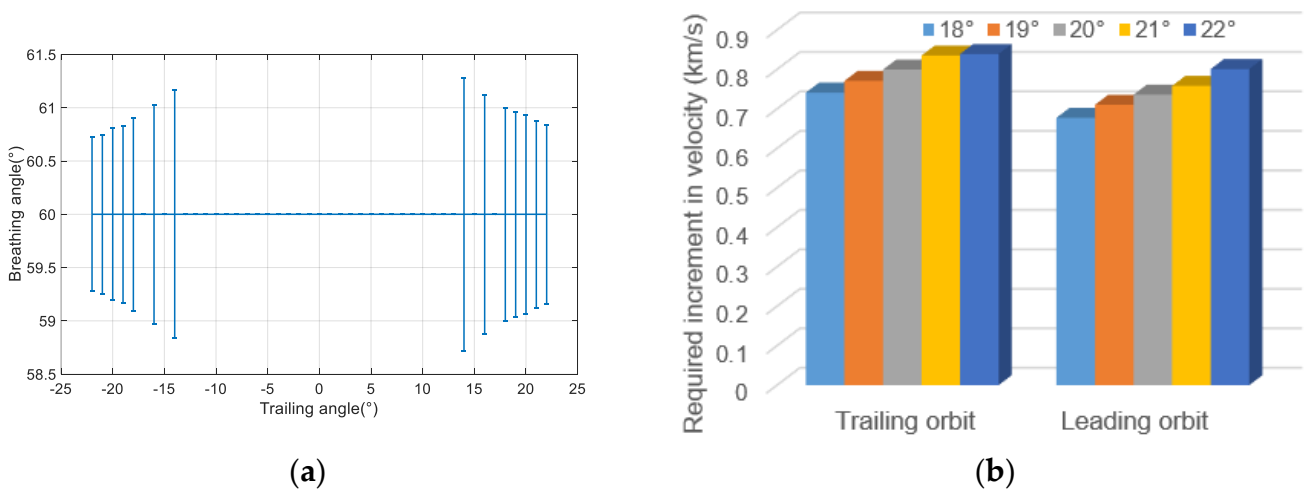


Figure 7. Cont.

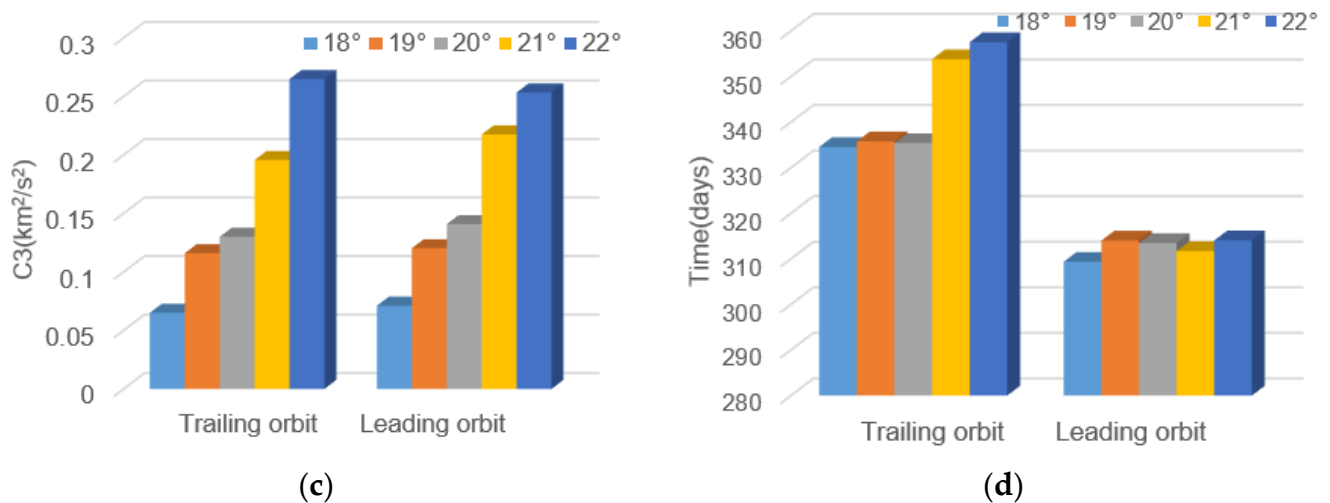


Figure 7. The effect of the initial trailing angle on the transfer orbit (the initial time of transfer is 1 April 2027). (a) The effect of the initial trailing angle on breathing angle; (b) the effect of the initial trailing angle on velocity increment; (c) the effect of the initial trailing angle on C3; (d) the effect of the initial trailing angle on transfer time.

(2) The effect of the initial phase angle of the formation on the transfer orbit

The initial phase angle of the formation affects the initial positions of the three satellites. In this section, the influence of the initial phase angle of the formation on the transfer orbit is explored. If the initial phase angle of satellite 1 is φ , the initial phase angles of satellites 2 and 3 are $\varphi + 120^\circ$ and $\varphi + 240^\circ$, respectively. As φ gradually increases from 10° to 120° , the outer circle of the formation triangle forms (Figure 8). C is the virtual center of the formation of the three satellites.

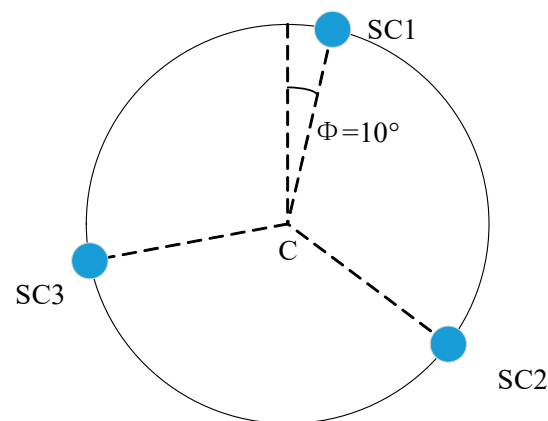


Figure 8. The initial phase angle of the formation.

Appendix A summarizes the designing results of the transfer orbit as the initial phase angle of SC1 changes from 10° to 120° on the first day of each month in 2026. In general, the design of the transfer orbit is influenced by the initial phase angle of the formation and the initial time of transfer. For instance, it can be seen from the images in Appendix A that for the Earth-trailing formation, the transfer orbit requires a smaller velocity increment when the initial phase angle is 10° or 20° from 1 January to 1 May 2026, and when the initial phase angle is 110° or 120° from 1 June to 1 November 2026. For the Earth-leading formation, a pattern opposite to that of the Earth-trailing formation is observed. Figure 9 shows the change in the velocity increments required by the three satellites with the initial phase angle of the formation on 1 January 2026. The three satellites require the smallest velocity increment when the initial phase angle is 10° for the Earth-trailing formation and

when the initial phase angle is 120° for the Earth-leading formation. Figure 10 shows the change in the velocity increment with the initial phase angle of the formation on 1 January 2027. The change pattern is similar to that on 1 January 2026.

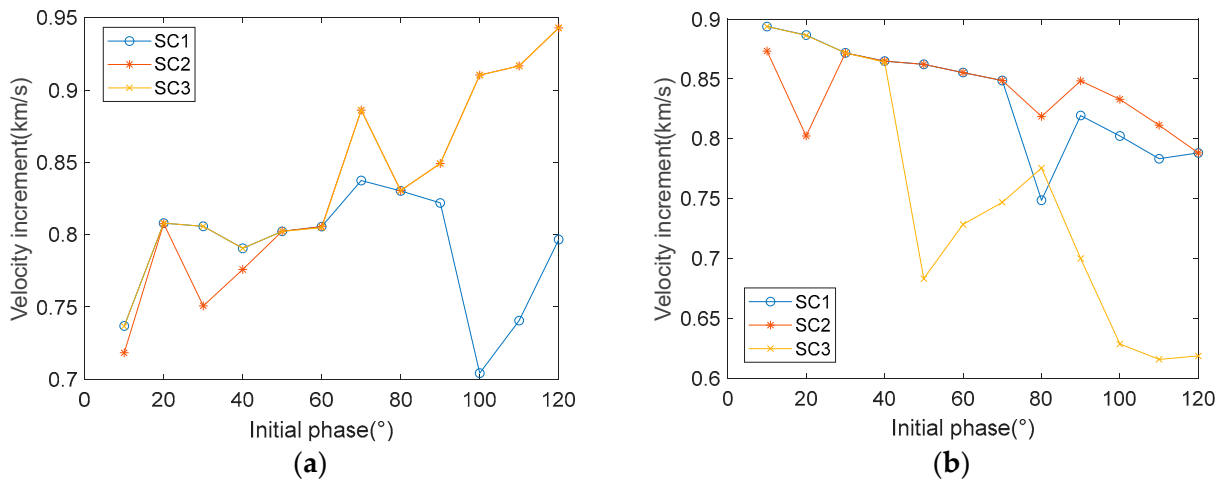


Figure 9. The effect of the initial phase angle on the transfer orbit (1 January 2026). (a) Trailing orbit; (b) leading orbit.

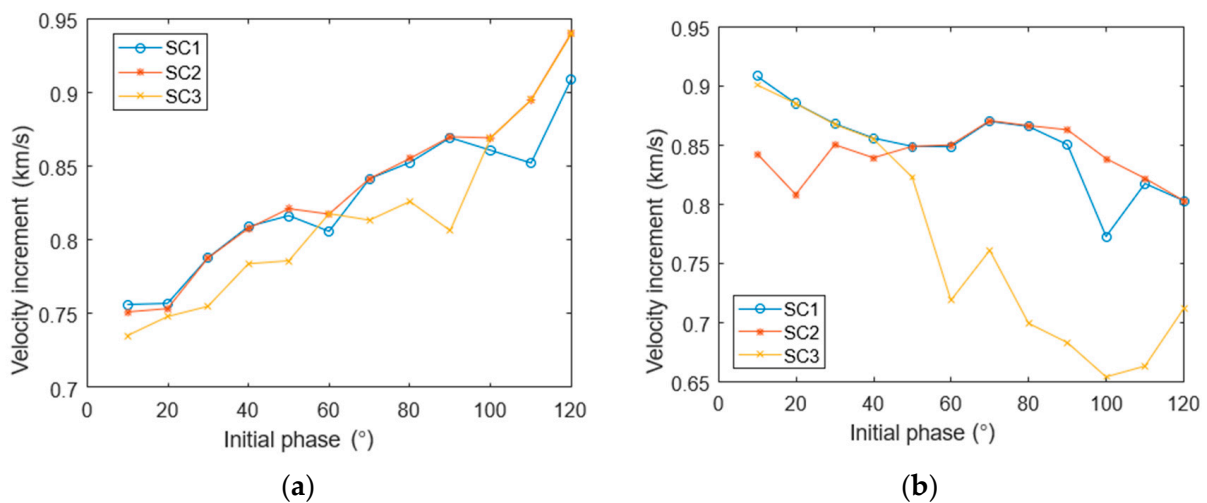


Figure 10. The effect of the initial phase angle on the transfer orbit (1 January 2027). (a) Trailing orbit; (b) leading orbit.

(3) The effect of the initial time of transfer on the transfer orbit

To investigate the relationship between the position of the satellites relative to Earth and the transfer orbit, the impulse transfer model is used for analysis. The change in the required velocity increment from the first day of the first month of 2026 to the first day of the last month of 2028 is shown in Figure 11. A smaller velocity increment is required from February to May in the Earth-leading formation, and from June to December in the Earth-trailing formation. To further explore the above patterns, the change in the required velocity increment every day throughout the year 2026 is analyzed (Figure 12). The required minimal velocity increments of the Earth-trailing and -leading formations are 0.6744 km/s and 0.7001 km/s, respectively.

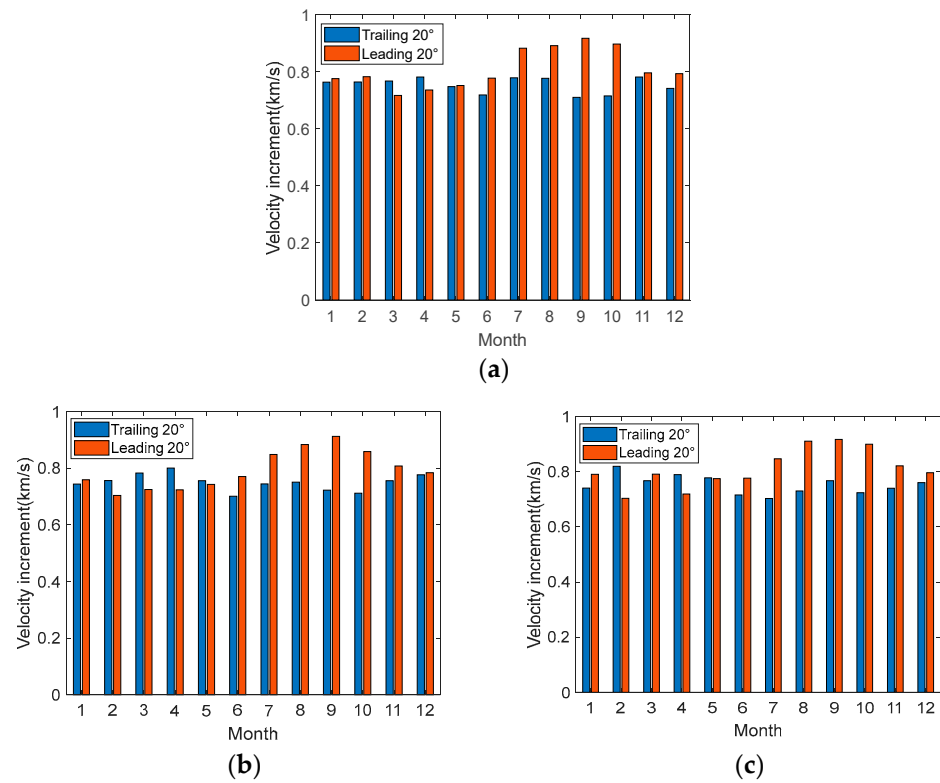


Figure 11. The required velocity increment from the first day of the first month of 2026 to the first day of the last month of 2028. (a) The required velocity increment of the first day of each month in 2026; (b) the required velocity increment of the first day of each month in 2027; (c) the required velocity increment of the first day of each month in 2028.

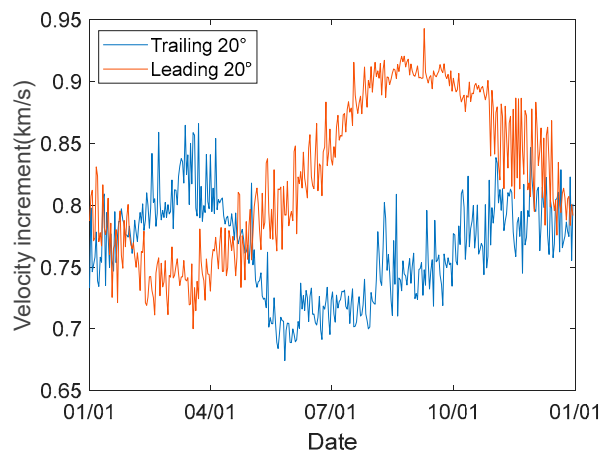


Figure 12. The required velocity increment everyday throughout the year of 2026.

5. Conclusions

In this paper, we provide the results of our study of the transfer orbit design of China’s heliocentric orbit space gravitational wave observatory for the first time. A space-based gravitational wave observatory transfer orbit is designed based on a two-impulse transfer model. Three optimization objectives are compared, which are the minimal total fuel consumption, the most uniform fuel consumption, and the minimal fuel consumption of each satellite. The minimal fuel consumption of each satellite is selected as the final optimization objective. The impulse transfer model is used to analyze the influence of the initial phase angle of the formation and the initial time of transfer on the transfer orbit. The Earth-leading and -trailing transfers show opposite patterns in the following three aspects.

(1) The influence of the initial phase angle of the formation on the transfer orbit.

The transfer orbit needs a smaller velocity increment when the initial phase angle is 10° or 20° from 1 January to 1 May 2026, and when the initial phase angle is 110° or 120° from 1 June to 1 November 2026 in the Earth-trailing formation. The Earth-leading formation shows an opposite pattern.

(2) The effect of the initial time of transfer on the transfer orbit.

A smaller velocity increment is required from February to May in the Earth-leading formation and from June to December in the Earth-trailing formation from 2026 to 2028.

(3) The impact of the initial trailing angle on the transfer orbit.

After taking into account the stability of the formation, C3, the required velocity increment, transfer time, and the distance to Earth, 20° is determined as the optimal initial trailing/leading angle.

Author Contributions: Conceptualization, Z.L.; methodology, Z.L.; software, Z.L.; validation, H.L.; formal analysis, H.L.; investigation, X.Z.; resources, X.Z.; data curation, X.Z.; writing—original draft preparation, Z.L.; writing—review and editing, H.L. and X.Z.; visualization, H.L. and X.Z.; supervision, Z.L.; project administration, Z.L.; funding acquisition, Z.L. All authors have read and agreed to the published version of the manuscript.

Funding: The work is sponsored by the Shanghai Sailing Program (Grant No. 23YF1444900).

Data Availability Statement: Data are contained within the article.

Conflicts of Interest: The authors declare no conflicts of interest.

Appendix A

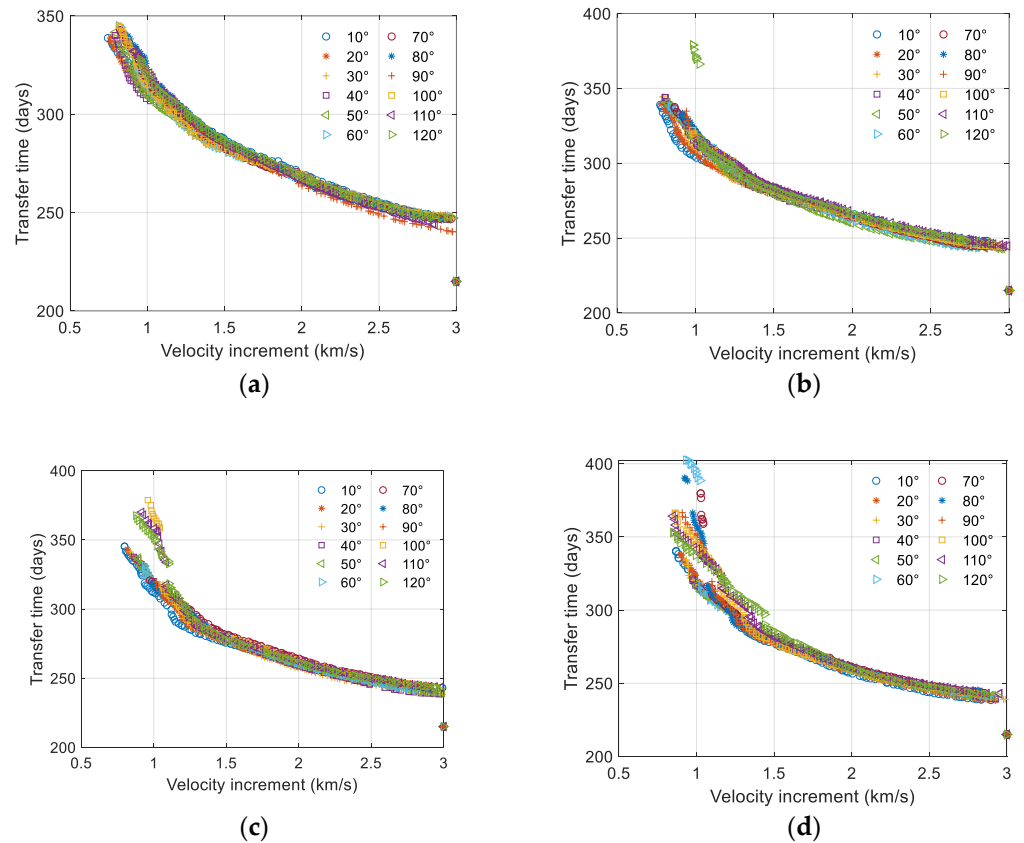


Figure A1. Cont.

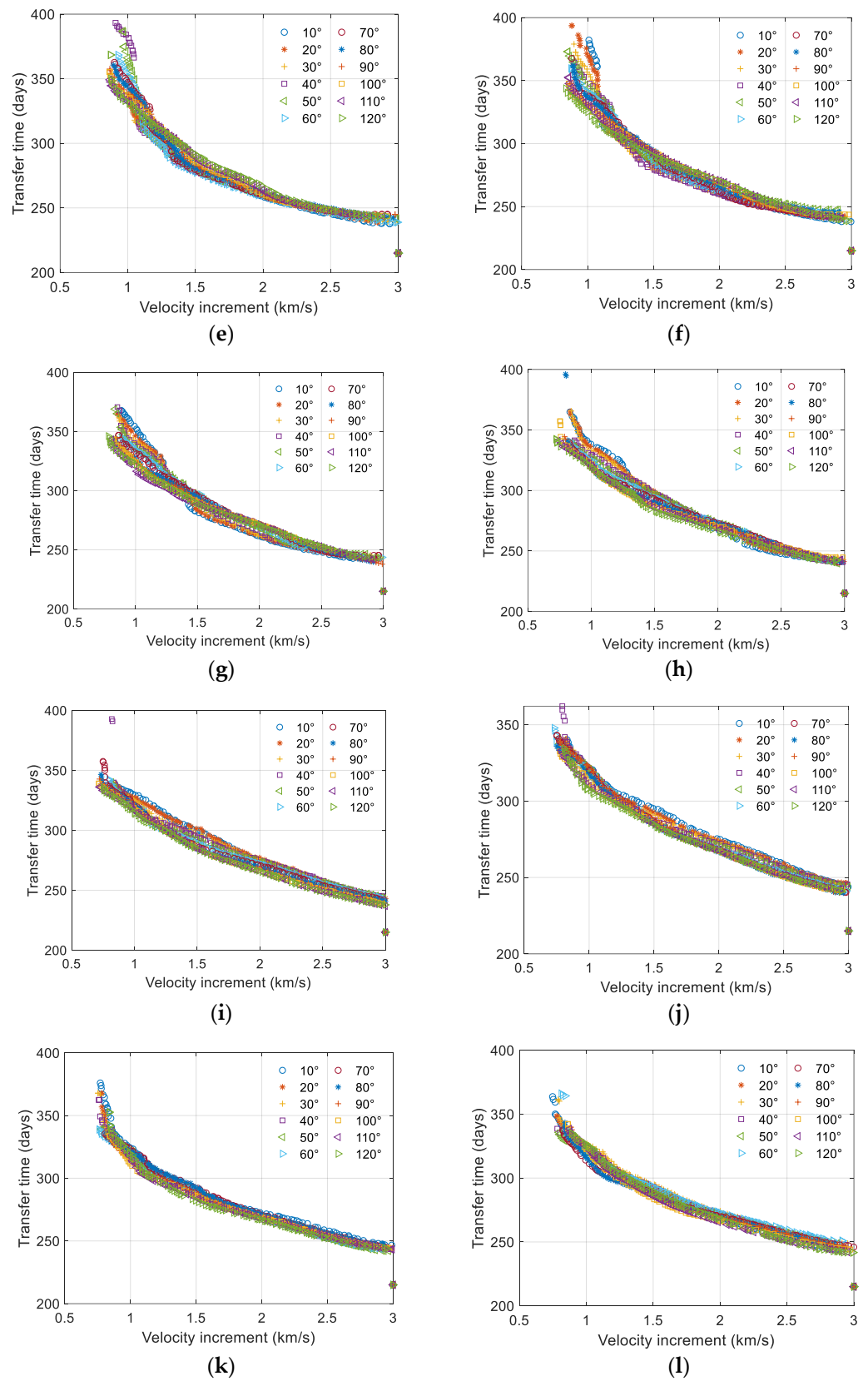


Figure A1. Initial phase’s effect on the transfer orbit (trailing orbit): (a) 1 January 2026; (b) 1 February 2026; (c) 1 March 2026; (d) 1 April 2026; (e) 1 May 2026; (f) 1 June 2026; (g) 1 July 2026; (h) 1 August 2026; (i) 1 September 2026; (j) 1 October 2026; (k) 1 November 2026; (l) 1 December 2026.

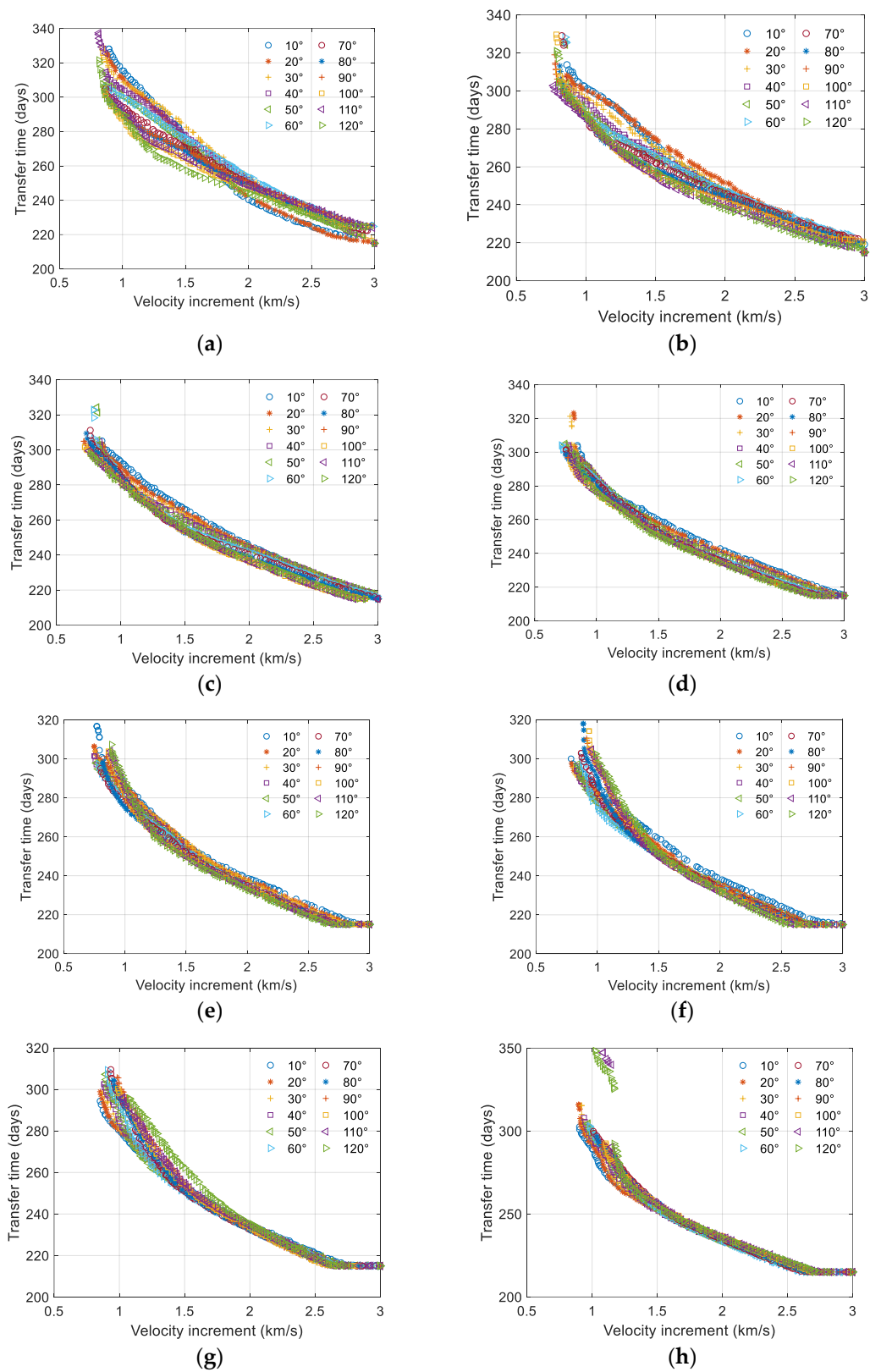


Figure A2. Cont.

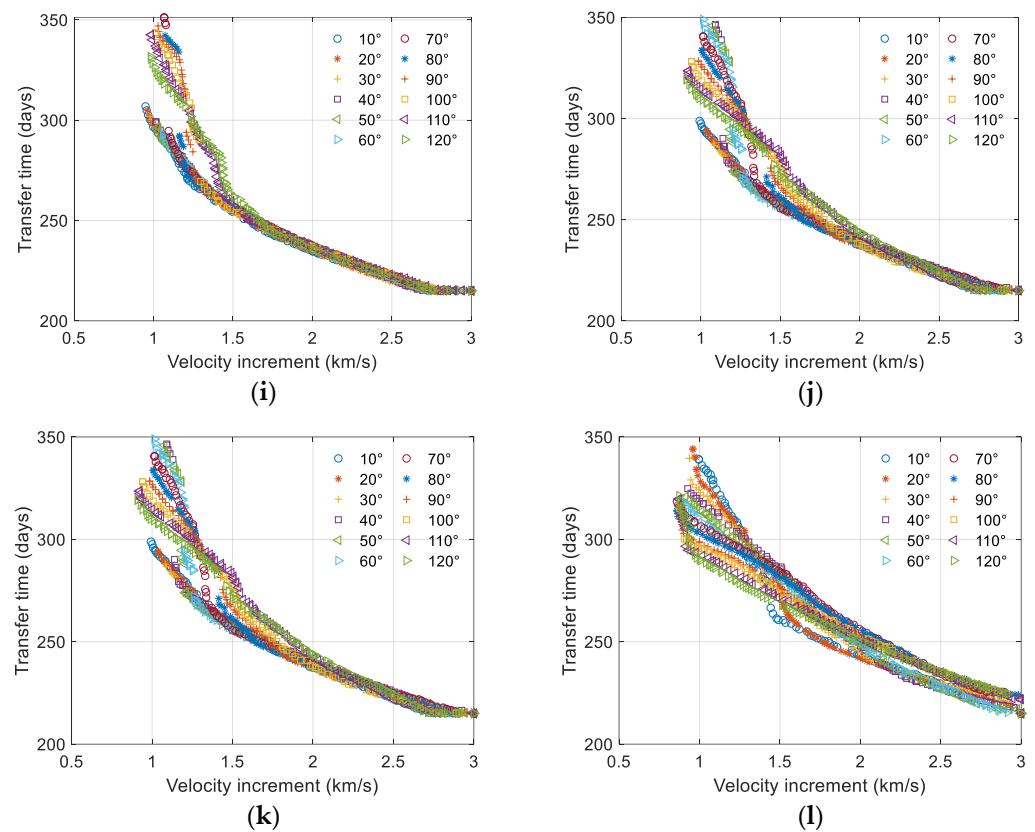


Figure A2. Initial phase's effect on the transfer orbit (leading orbit): (a) 1 January 2026; (b) 1 February 2026; (c) 1 March 2026; (d) 1 April 2026; (e) 1 May 2026; (f) 1 June 2026; (g) 1 July 2026; (h) 1 August 2026; (i) 1 September 2026; (j) 1 October 2026; (k) 1 November 2026; (l) 1 December 2026.

References

- Abbott, B.P.; Abbott, R.; Adhikari, R.; Ajith, P.; Allen, B.; Allen, G.; Amin, R.S.; Anderson, S.B.; Anderson, W.G.; A Arain, M.; et al. LIGO: The laser interferometer gravitational-wave observatory. *Rep. Prog. Phys.* **2009**, *72*, 7. [\[CrossRef\]](#)
- Abbott, B.P.; Abbott, R.; Abbott, T.D.; Acernese, F.; Ackley, K.; Adams, C.; Adams, T.; Addesso, P.; Adhikari, R.X.; Adya, V.B.; et al. GW170817: Implications for the stochastic gravitational-wave background from compact binary coalescences. *Phys. Rev. Lett.* **2018**, *120*, 091101. [\[CrossRef\]](#) [\[PubMed\]](#)
- Cornish, N.J.; Rubbo, L.J. LISA response function. *Phys. Rev. D* **2003**, *67*, 022001. [\[CrossRef\]](#)
- Nayak, K.R.; Koshti, S.; Dhurandhar, S.V.; Vinet, J.Y. On the minimum flexing of LISA's arms. *Class. Quantum Gravity* **2006**, *23*, 1763. [\[CrossRef\]](#)
- Pucacco, G.; Bassan, M.; Visco, M. Autonomous perturbations of LISA orbits. *Class. Quantum Gravity* **2010**, *27*, 235001. [\[CrossRef\]](#)
- Li, G.; Yi, Z.; Heinzl, G.; Rüdiger, A.; Jennrich, O.; Wang, L.; Xia, Y.; Zeng, F.; Zhao, H. Methods for Orbit Optimization for the Lisa Gravitational Wave Observatory. *Int. J. Mod. Phys. D* **2008**, *17*, 1021–1042. [\[CrossRef\]](#)
- Li, Z.; Zheng, J. Orbit determination for a space-based gravitational wave observatory. *Acta Astronaut.* **2021**, *185*, 170–178. [\[CrossRef\]](#)
- Li, Z.; Zheng, J.; Li, M. Orbit insertion error analysis for a space-based gravitational wave observatory. *Adv. Space Res.* **2020**, *67*, 3744–3754. [\[CrossRef\]](#)
- Luo, Z.; Guo, Z.; Jin, G.; Wu, Y.; Hu, W. A brief analysis to Taiji: Science and technology. *Results Phys.* **2019**, *16*, 102918. [\[CrossRef\]](#)
- Luo, Z.; Liu, H.; Jin, G. The recent development of interferometer prototype for Chinese gravitational wave detection pathfinder mission. *Opt. Laser Technol.* **2018**, *105*, 146–151. [\[CrossRef\]](#)
- Mei, J.; Bai, Y.-Z.; Bao, J.; Barausse, E.; Cai, L.; Canuto, E.; Cao, B.; Chen, W.-M.; Chen, Y.; Ding, Y.-W.; et al. The TianQin project: Current progress on science and technology. *Prog. Theor. Exp. Phys.* **2020**, *2021*, 05A107. [\[CrossRef\]](#)
- Liang, Z.-C.; Hu, Y.-M.; Jiang, Y.; Cheng, J.; Zhang, J.-D.; Mei, J. Science with the TianQin Observatory: Preliminary results on stochastic gravitational-wave background. *Phys. Rev. D* **2022**, *105*, 022001. [\[CrossRef\]](#)
- Ye, B.-B.; Zhang, X.; Zhou, M.-Y.; Wang, Y.; Yuan, H.-M.; Gu, D.; Ding, Y.; Zhang, J.; Mei, J.; Luo, J. Optimizing orbits for TianQin. *Int. J. Mod. Phys. D* **2019**, *28*, 1950121. [\[CrossRef\]](#)
- Hu, X.-C.; Li, X.-H.; Wang, Y.; Feng, W.-F.; Zhou, M.-Y.; Hu, Y.-M.; Hu, S.-C.; Mei, J.-W.; Shao, C.-G. Fundamentals of the orbit and response for TianQin. *Class. Quantum Gravity* **2018**, *35*, 095008. [\[CrossRef\]](#)

15. Tan, Z.; Ye, B.; Zhang, X. Impact of orbital orientations and radii on TianQin constellation stability. *Int. J. Mod. Phys. D* **2020**, *29*, 2050056. [[CrossRef](#)]
16. Xia, Y.; Li, G.; Heinzl, G.; Rüdiger, A.; Luo, Y. Orbit design for the Laser Interferometer Space Antenna (LISA). *Sci. China Phys. Mech. Astron.* **2010**, *53*, 179–186. [[CrossRef](#)]
17. Sweetser, T.H. An end-to-end trajectory description of the LISA mission. *Class. Quantum Gravity* **2005**, *22*, S429–S435. [[CrossRef](#)]
18. Joffre, E.; Wealthy, D.; Fernandez, I.; Trenkel, C.; Voigt, P.; Ziegler, T.; Martens, W. LISA: Heliocentric formation design for the laser interferometer space antenna mission. *Adv. Space Res.* **2020**, *67*, 3868–3879. [[CrossRef](#)]
19. Wang, G.; Ni, W.T.; Wu, A.M. Orbit design and thruster requirement for various constant arm space mission concepts for gravitational-wave observation. *Int. J. Mod. Phys. D* **2020**, *29*, 1940006. [[CrossRef](#)]
20. Wu, A.-M.; Ni, W.-T. Deployment and simulation of the ASTROD-GW formation. *Int. J. Mod. Phys. D* **2013**, *22*, 1341005. [[CrossRef](#)]
21. Hellings, R. *JPL Team X Space-Based Gravitational Wave Observatory OMEGA Report*; California Institute of Technology: Los Angeles, CA, USA, 2012.
22. Giulicchi, L.; Wu, S.-F.; Fenal, T. Attitude and orbit control systems for the LISA Pathfinder mission. *Aerosp. Sci. Technol.* **2013**, *24*, 283–294. [[CrossRef](#)]
23. Zhang, J.; Dai, H.; Dang, Z.; Yue, X. Research on configuration design and initialization method of near-Earth gravitational wave formation. *Chin. J. Appl. Mech.* **2023**, *40*, 1249–1256.

Disclaimer/Publisher’s Note: The statements, opinions and data contained in all publications are solely those of the individual author(s) and contributor(s) and not of MDPI and/or the editor(s). MDPI and/or the editor(s) disclaim responsibility for any injury to people or property resulting from any ideas, methods, instructions or products referred to in the content.